Fine Chemical Engineering
https://ojs.wiserpub.com/index.php/FCE/

Research Article

Rapid Flash-Paper Combustion Synthesis of Titania and Carbon Pigments

Athanasios B. Bourlinos[1*], Dimitrios Moschovas[2], Apostolos Avgeropoulos[2], Theofanis N. Maimaris[2], Constantinos E. Salmas[2], Michael A. Karakassides[2]

[1]Physics Department, University of Ioannina, Ioannina, 45110, Greece
[2]Department of Materials Science & Engineering, University of Ioannina, Ioannina, 45110, Greece
E-mail: bourlino@uoi.gr

Received: 12 January 2026; **Revised:** 26 February 2026; **Accepted:** 5 March 2026

Graphical Abstract:

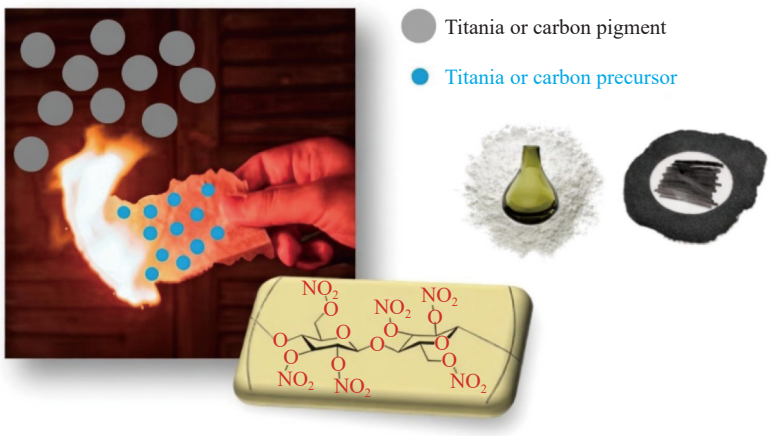

Abstract: Flash-paper combustion offers a rapid, energy-efficient route for synthesizing industrially relevant pigments. In this study, we demonstrate the preparation of titania and carbon pigments using nitrocellulose-based flash paper as a reactive scaffold. For titania, flash paper was impregnated with an aqueous Ti(III) chloride solution, dried, and ignited, yielding a lightweight product composed of anatase and rutile phases, which was subsequently further calcined to obtain nearly pure rutile. The resulting pigment effectively modified the color of lead borate glass, highlighting its practical applicability. The carbon pigment was similarly produced by impregnating flash paper with a sugar solution, followed by ignition. When incorporated into waterborne acrylic ink, the black pigment formed uniform, flexible coatings, demonstrating its functional performance in ink formulations. Flash-paper combustion is a rapid, energy self-sufficient, and potentially scalable method for producing high-value titania and carbon pigments in a simple, sustainable process that can harness the released thermal energy.

DOI: https://doi.org/10.37256/fce.7120269592

***Keywords*:** flash-paper, pigments, rapid combustion, scalable synthesis, thermal energy

1. Introduction

Titania (titanium dioxide, TiO_2) and carbon pigments are among the most widely used commercial pigments due to their excellent color strength, chemical stability, and broad versatility. Together, these materials form the backbone of modern pigmentation technologies, supporting applications ranging from consumer goods and building materials to specialty industrial products.

Titania is an important pigment,[1,2] owing to its high refractive index, excellent light-scattering properties, chemical stability, and low toxicity, especially in the rutile form. Consequently, paints and glass together account for approximately 4 million tonnes of TiO_2 consumption each year.

Industrial TiO_2 production is largely driven by the sulfate and chloride processes, both of which use ilmenite ore as a Ti(IV) source.[1-3] In addition to these well-established methods, a range of newer synthesis approaches has been developed, primarily based on Ti(IV) and, to a lesser extent, Ti(III) precursors.[4-9] The sol-gel method relies on hydrolysis and condensation of titanium alkoxides to generate a colloidal network that yields TiO_2 after drying and calcination. Hydrothermal synthesis employs elevated temperature and pressure to produce crystalline phases with controlled morphologies. Direct oxidation converts titanium metal to TiO_2 under carefully regulated conditions. Chemical vapor deposition forms thin TiO_2 films through thermal decomposition of volatile titanium species. Sonochemical synthesis uses ultrasonic cavitation to drive rapid nucleation and particle growth, whereas microwave-assisted methods provide fast, energy-efficient, and uniform heating. In solution combustion synthesis, a titanium precursor reacts exothermically with a fuel—such as urea, glycine, or citric acid—to rapidly form titania. Flame-spray pyrolysis similarly generates TiO_2 by injecting a precursor-laden solution into a high-temperature flame. More recently, hypergolic synthesis has emerged as a novel route, where suitable precursors react spontaneously with fuming nitric acid under ambient conditions, enabling the instant formation of photocatalytic titania. Finally, high-energy ball milling is capable of altering particle size, crystallinity, and optical properties through intensive grinding and mechanochemical activation.

On the other hand, carbon pigments provide high tinting strength, a deep and long-lasting black coloration, and an exceptional stability. As a result, global production of carbon pigments for paints and inks is on the order of one million tonnes per year—slightly lower than, yet approaching, that of titania.[1] Industrially, the pigment is obtained by pyrolyzing hydrocarbons under low-oxygen conditions. When the hydrocarbon feedstock is heated to high temperatures with insufficient oxygen for incomplete combustion, it breaks down into fine carbon particles.[1,10] Meanwhile, sugars and biomass have emerged as promising and cost-effective feedstocks for producing carbon pigments from readily available sources.[11-13]

Our group recently introduced a versatile synthesis approach known as flash-paper combustion, previously demonstrated for a range of pigments including cobalt blue ($CoAl_2O_4$), chromium oxide green (Cr_2O_3), and black magnetic spinels.[14] Flash paper, composed of nitrocellulose, burns extremely rapidly and leaves no solid residue. At the same time, its highly porous, fibrous structure allows remarkably uniform precursor uptake simply by wetting the sheet with an aqueous precursor solution. Once dried, a single ignition triggers a self-sustaining exothermic reaction that completes within seconds without any external heat input, yielding the desired material. The method's simplicity and energy efficiency highlight strong prospects for industrial-scale expansion.

Building on this earlier work, and emphasizing the general applicability of the method, we now demonstrate the synthesis of TiO_2 and carbon pigments *via* flash-paper combustion. In the first case, flash paper is soaked in an aqueous solution of a Ti(III) salt. The choice of Ti(III) allows the precursor to penetrate deeply and uniformly into the paper, as its slow oxidation forms well-anchored TiO_2 and prevents the premature precipitation or surface-limited deposition typical of Ti(IV) sources.[15] After drying, the paper is ignited in air, and its rapid combustion converts the embedded precursor into titania. In the second case, carbon is produced by soaking flash paper in an aqueous table-sugar solution, which serves as the carbon source. Once the sugar-impregnated sheet is dried and ignited, the sugar undergoes rapid thermal decomposition, leaving behind carbon. For indicative and technical purposes, titania was used as a colorant in lead borate glass, while carbon served as an additive in black ink formulations. The potential for scaling up the method for industrial pigment production is also discussed.

2. Materials and methods

2.1 *Flash-paper combustion synthesis of titania and carbon pigments*

A solution containing 15% titanium(III) chloride in 10% HCl (Merck) was used as the titania precursor. Rectangular pieces of thick nitrocellulose flash paper (6 cm × 12 cm; MagicStar, Keratsini, Greece) were immersed in the solution for a few seconds, then removed and allowed to drain. The drained pieces were suspended with small wooden clips and dried in an oven at 90 °C for 10 min. The dried samples were then ignited in a porcelain crucible using a lighter, triggering rapid, self-sustained combustion. Within a few seconds, this process produced a lightweight titania pigment, with a typical yield of approximately 10 mg per flash paper piece.

A second solution was prepared by dissolving 40 g of table sugar in 100 mL of deionized water. Flash paper pieces of identical dimensions were immersed in the sugar solution, removed, drained, and suspended with wooden clips, then dried in an oven at 90 °C for 45 min. Upon ignition, the dried sheets underwent rapid combustion, yielding lightweight carbon within a few seconds, with an approximate yield of 5 mg per flash paper piece.

Note that the flash paper used in this work is the commercially available type intended for magic tricks and stage effects. It is formulated to burn rapidly without producing an explosive hazard under normal handling and use.

2.2 *Characterization techniques*

X-Ray Diffraction (XRD) measurements were carried out on a Bruker D8 Advance diffractometer (Bruker AXS GmbH, Karlsruhe, Germany) with Cu Kα radiation (λ = 1.54 Å), using a silicon background-free holder. Raman spectra were recorded with a micro-Raman system RM 1,000 Renishaw using a laser excitation line at 532 nm (10 mW). X-ray Photoelectron Spectroscopy (XPS) measurements were performed in an ultra-high vacuum at a base pressure of 4×10^{-10} mbar with a SPECS GmbH spectrometer equipped with a monochromatic Mg Kα source ($h\nu$ = 1,253.6 eV) and a Phoibos-100 hemispherical analyzer (Berlin, Germany). The spectral analysis included a Shirley background subtraction and peak deconvolution with mixed Gaussian-Lorentzian functions using a least-squares curve-fitting program (WinSpec, University of Namur, Belgium). Transmission Electron Microscopy (TEM) observations were performed using a JEM HR-2100 microscope (JEOL Ltd., Tokyo, Japan) operated at 200 kV in bright-field mode. A drop of ethanol containing ultrasonically dispersed particles was placed onto a TEM grid (CF300-CU-UL, 300-mesh from Electron Microscopy Sciences, Hatfield, UK) and air-dried at room temperature. Nitrogen (N_2) adsorption-desorption isotherms were measured using an ASAP 2460 analyzer (Micromeritics, Norcross, GA, USA) with ultrahigh purity N_2 (99.999%). The samples were outgassed for 10 h under vacuum (10^{-4} mbar) at 120 °C. Isotherms were recorded at 77 K using a liquid N_2 Dewar vessel at relative Pressures (P/P_o) ranging from 10^{-2} to 0.99, and the specific surface areas were calculated using the Brunauer-Emmett-Teller (BET) method.

2.3 *Preparation of base and titania-doped lead borate glasses*

A PbO-B_2O_3-ZnO glass was prepared by thoroughly homogenizing PbO, H_3BO_3, and ZnO in the proportions 2.0 g, 1.2 g, and 0.2 g, respectively. The blended powder was placed in a porcelain crucible and subjected to high-temperature melting at 900 °C for 20 min in air, after which the molten mixture was cooled to room temperature, yielding the base glass. For the titania-doped sample, 0.2 g of TiO_2—corresponding to 7.5 mol % Ti relative to the total cations—was incorporated into the initial batch prior to melting. The sample then underwent the same thermal treatment to obtain the Ti-containing glass.

2.4 *Carbon ink preparation*

The carbon ink was prepared by dispersing 0.15 g of carbon powder in 0.5 mL of deionized water and 1.0 mL of acrylic medium (Royal Talens 012 GLOSS, Amsterdam). The mixture was transferred to a glass vial and sonicated in an ultrasonic bath to ensure thorough dispersion of the carbon particles and homogenization of the ink, resulting in a formulation containing 10% pigment.

3. Results and discussion

3.1 *Synthesis, characterization, and application of titania pigment*

A commercially sourced aqueous titanium(III) chloride solution served as the TiO_2 precursor.[16] Rectangular pieces of flash paper were soaked in the solution and then dried. During drying, partial oxidation of purple Ti(III) to colorless Ti(IV) occurred, imparting a faint purple hue to the paper. When ignited, the material underwent a rapid, self-propagating combustion reaction, which can be approximated by the following balanced equations (using the average nitrocellulose composition $C_6H_{7.6}O_{8.4}N_{2.4}$):[17]

$$74\ TiCl_3 + 10\ C_6H_{7.6}O_{8.4}N_{2.4} + 111\ O_2 \rightarrow 74\ TiO_2 + 12\ N_2 + 60\ CO_2 + 38\ H_2O + 111\ Cl_2 \quad (1)$$

$$TiCl_4 + 10\ C_6H_{7.6}O_{8.4}N_{2.4} + 38\ O_2 \rightarrow TiO_2 + 60\ CO_2 + 38\ H_2O + 12\ N_2 + 2\ Cl_2 \quad (2)$$

Within seconds, the process yielded a lightweight solid exhibiting the characteristic coloration of the pigment (Figure 1).

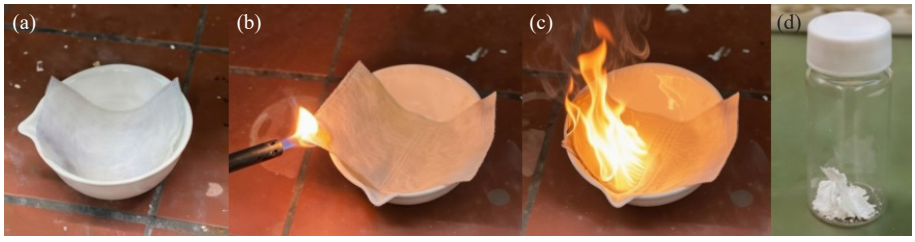

Figure 1. From left to right: (a) flash paper after impregnation and drying, showing a pale purple tint due to Ti(III); (b) ignition of the impregnated paper; (c) rapid, self-sustained combustion producing titania; and (d) the collected lightweight TiO_2 solid after combustion

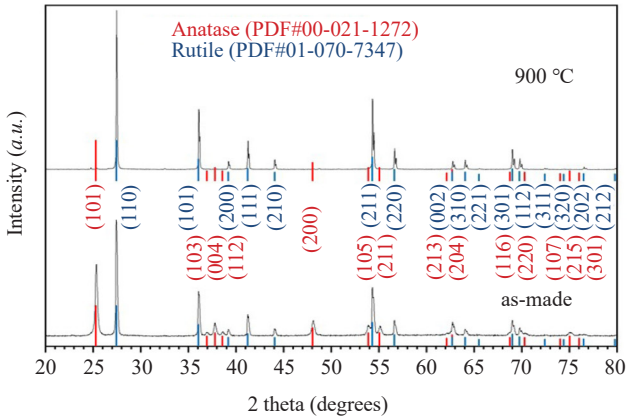

Figure 2. XRD patterns of the as-made titania powder and the sample calcined at 900 °C, shown with reference peak positions for anatase (red, PDF#00-021-1272) and rutile (blue, PDF#01-070-7347). The as-made material contains a mixture of anatase and rutile, whereas calcination at 900 °C shifts the phase composition toward rutile

The XRD pattern of the as-made titania (Figure 2, lower) displays reflections from both anatase and rutile, consistent with the Rietveld refinement showing a composition of 36% anatase and 64% rutile. Ti(III) favors the anatase phase because oxygen vacancies introduced by its presence are better accommodated in the less dense, more flexible lattice. In contrast, Ti(IV), which does not generate such vacancies, stabilizes the more compact rutile structure. Phase formation thus reflects a competition between lattice density and defect accommodation: anatase is stabilized by Ti(III)-

induced defects, while rutile is favored by the tendency toward a dense, defect-free lattice. In mixed-valence Ti(III)/Ti(IV) systems, this competition results in the coexistence of both anatase and rutile phases.

In general, rutile is strongly favored over anatase in coloring applications due to its superior opacity, higher refractive index and density, as well as enhanced weather resistance and durability. To obtain a rutile-grade pigment, the mixture required calcination at an elevated temperature. Usually, the conversion of anatase to rutile begins irreversibly at roughly 600 °C and progresses to completion only at higher temperatures, with the duration of heating playing a critical role in achieving full transformation.[18] Mechanistically, this transformation involves nucleation of rutile within the anatase matrix, followed by growth driven by lattice rearrangement and densification. Accordingly, when the sample was calcined at 900 °C for 2 h—well above 600 °C—it exhibited marked changes in phase composition, even though the overall peak widths and intensities remain largely similar. Thus, while the diffraction pattern of the calcined titania showed only subtle sharpening, the phase composition underwent a pronounced shift (Figure 2, upper). Rietveld analysis revealed that the calcined material consisted of 99.5% rutile and only 0.5% anatase, demonstrating that high-temperature treatment drove an almost complete transformation to the rutile phase. The N_2 surface area was determined to be 18 $m^2 \cdot g^{-1}$.

TEM analysis of the rutile phase reveals the coexistence of two distinct titania morphologies. One population consists of irregularly shaped titania nanoparticles,[19] in which the individual particles are submicron in size and tend to form densely packed aggregates (Figure 3a). The second population is composed of plate-like titania nanosheets[20] with a layered structure[21] and lateral dimensions also in the submicron range (Figure 3b). Both morphologies are present in nearly equal proportions, with an approximate 50:50 distribution between nanoparticle aggregates and nanosheets.

It appears that ignition of titanium chloride-impregnated flash paper produces TiO_2 through two parallel formation routes. The lamellar paper matrix acts as a sacrificial template,[22] preserving a sheet-like morphology, while volatile titanium chlorides undergo thermal decomposition to generate irregular or nearly spherical particles.[23] It should be noted that in our previous work,[14] cobalt blue formed nanoscale spheres due to nucleation within transient molten droplets originating from low-melting precursor nitrate salts. In contrast, TiO_2 derived from titanium chlorides in the present case forms predominantly *via* solid-state and gas-phase growth, resulting in distinct particle morphologies and size distributions. Although not systematically investigated, the thickness of the flash paper, whether thin or thick, may also influence particle size and morphology and thus cannot be ruled out. Other factors, including reaction temperature, the surrounding atmosphere, precursor concentration, and possible post-formation transformations such as sintering or coalescence, may also play a role and warrant further study.

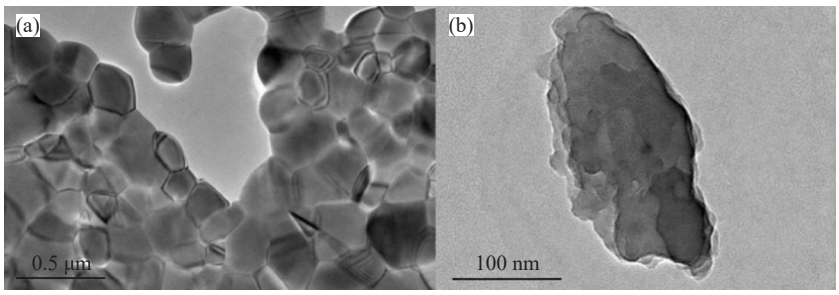

Figure 3. TEM images of the rutile phase, showing (a) aggregates of irregular nanoparticles and (b) plate-like nanosheets

In addition to its role as a pigment in paints, titania is also used to color glass, regardless of whether it is in the anatase or rutile form, as both dissolve during melting. As such, global use of TiO_2 in glass pigmentation is roughly 50 thousand tonnes per year. The coloration mechanism is governed by titanium ions incorporated into the melt, where they modify optical absorption.

PbO-B_2O_3-ZnO glasses are low-melting lead borate compositions modified with zinc oxide to enhance chemical durability and mechanical strength while maintaining high transparency. They typically soften at temperatures far below those of conventional silicate glasses,[24,25] enabling easier processing and more energy-efficient manufacturing. These glasses often show a yellowish tint (Figure 4a), originating from Ultraviolet (UV)-edge absorption by mixed-valence

Pb^{2+}/Pb^{4+} ions.[26] Owing to their low-temperature processability and tunable optical properties, they are employed in optical components, electronic substrates, sealing materials, radiation-shielding, and specialty coatings.

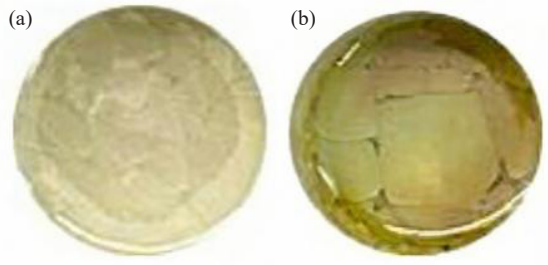

Figure 4. Visual comparison of lead borate glasses: undoped sample (a) and titania-doped sample (b), showing the noticeable color change induced by Ti addition

Titania produced *via* flash-paper combustion was used as a proof-of-concept functional additive to modify the color of lead borate glass. When 7.5 mol % TiO_2 was added to PbO-B_2O_3-ZnO glass, an olive green tint was observed (Figure 4b). The color develops because TiO_2 modifies the glass network and the light-absorption behavior of lead ions, shifting the transmitted hue from yellow toward olive green. In addition, Ti^{4+} ions contribute their own coloration through strong $O^{2-} \rightarrow Ti^{4+}$ charge-transfer transitions, with further contributions from intervalence charge transfer when small amounts of Ti^{3+} are present.[27] Similar shifts in color, but from colorless to yellow, have likewise been observed in titania-doped silicate glasses.[28-30] On the other hand, the Ti content of 7.5 mol % was chosen as a representative value within the range reported for titania-doped glasses (*ca.* 5-10%),[31] as it also produces a noticeable color change without phase separation.

3.2 *Synthesis, characterization, and application of carbon pigment*

An aqueous solution of table sugar was employed as the carbon source.[32,33] Sheets of flash paper were immersed in this solution and subsequently allowed to dry. As the solvent evaporated, the treated paper developed a greenish tint, attributed to the formation of nitroso-modified sugar species.[34,35] This likely arises from a mild nitrosation process in which nitrocellulose releases trace nitrosating species (e.g., NO^+/HONO/NO_2^-) that react with the sugar to form nitroso-substituted derivatives. Ignition triggered a fast, self-propagating combustion event, summarized by the approximate overall equation below:

$$C_{12}H_{22}O_{11} + 10\ C_6H_{7.6}O_{8.4}N_{2.4} \rightarrow 49\ C + 12\ N_2 + 49\ H_2O + 23\ CO_2 \quad (3)$$

The reaction concluded within seconds, leaving behind a lightweight carbon solid (Figure 5). A specific surface area of 55 $m^2 \cdot g^{-1}$ was obtained from N_2 porosimetry.

Figure 5. From left to right: (a) treated flash paper with a greenish hue attributed to nitroso-sugar formation; (b) ignition of the treated sheet; (c) rapid, self-propagating combustion yielding carbon; and (d) the resulting lightweight carbon solid

The material was characterized by XRD and Raman techniques, which revealed the signature features of amorphous carbon. The XRD pattern in the left panel of Figure 6 exhibits the broad, low-intensity diffraction feature typical of amorphous carbon, reflecting the absence of long-range ordering.[36] The wide (002) hump centered around $2\theta \approx 23\text{-}25°$ corresponds to an interlayer spacing of approximately 0.387 nm, which is larger than that of crystalline graphite (0.335 nm) and indicative of turbostratic or highly disordered carbon layers. Notably, a sharp (002) reflection protrudes from the top of this broad halo, suggesting the presence of a minor fraction of more ordered domains or locally stacked graphitic layers embedded within the predominantly amorphous matrix. This sharp peak does not dominate the pattern but stands out enough to indicate heterogeneous structural ordering.[37] Moreover, the weak, broad peak near 43°—often attributed to the graphite (101) plane—further supports the presence of small, locally ordered graphitic domains.[36] Consistent with the XRD results, the Raman spectrum in the right panel of the same figure displays characteristic D and G bands at 1,329 cm^{-1} and 1,582 cm^{-1}, respectively.[38] The strong and broadened D band highlights a high concentration of defects and a disordered carbon network, while the G band reflects the stretching vibrations of sp^2-bonded carbon atoms. The significant D/G intensity ratio and peak broadening confirm limited graphitic domain size and substantial structural disorder, supporting the interpretation of an essentially amorphous carbon material with small, locally ordered regions.

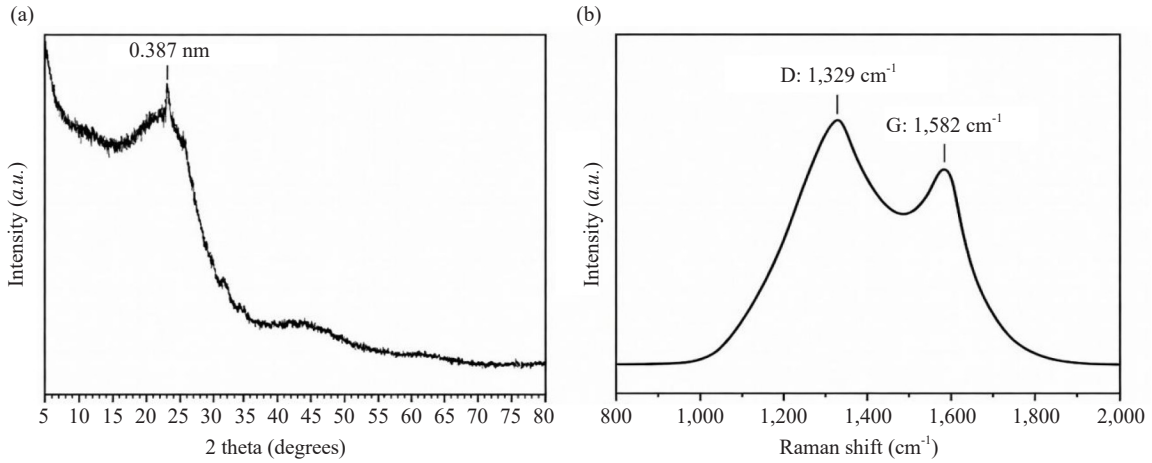

Figure 6. XRD pattern (a) and Raman spectrum (b) of the derived carbon

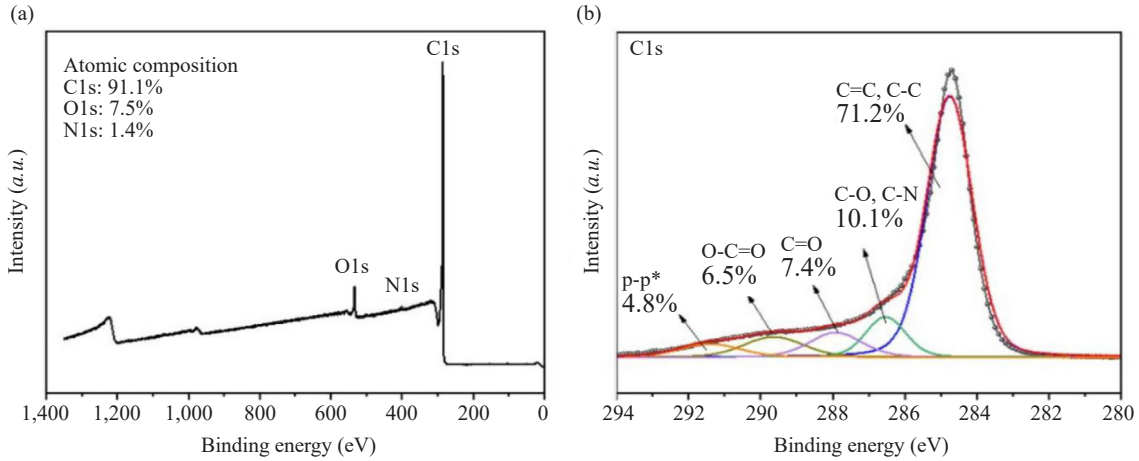

Figure 7. XPS spectra of the carbon sample. (a) The left panel shows the survey spectrum with C1s, O1s, and N1s peaks. (b) The right panel displays the high-resolution C1s spectrum with peak deconvolution

The XPS survey spectrum confirms the elemental composition and surface chemistry of the sample (Figure 7a). As shown in the wide-scan spectrum, the material is predominantly composed of carbon, with a strong C1s signal, accompanied by weaker O1s and N1s peaks. Quantitative analysis indicates atomic percentages of 91.1% C, 7.5% O, and 1.4% N, demonstrating that the surface is largely carbonaceous with a minor contribution from oxygen- and nitrogen-containing functional groups. To further elucidate the carbon bonding configuration, high-resolution spectra of the C1s region were deconvoluted into multiple components (Figure 7b). The dominant peak at 284.6 eV, accounting for 71.2% of the total C1s area, is attributed to C-C and C=C bonds, indicating that graphitic or sp^2/sp^3-hybridized carbon constitutes the primary framework of the material. A secondary component at 286.4 eV (10.1%) corresponds to C-O and C-N functionalities. Additional contributions at 287.7 eV (7.4%) and 288.8 eV (6.5%) are assigned to C=O and O-C=O species, respectively, suggesting the existence of carbonyl and carboxyl/ester groups. A weak p-p* satellite peak at 291-292 eV (4.8%) further supports the presence of conjugated aromatic structures within the carbon matrix.

TEM reveals two distinct carbon morphologies. The dominant population consists of plate-like carbon nanosheets[39] with lateral dimensions in the submicron range (Figure 8a). In addition, aggregates of nearly spherical carbon particles are observed,[40] where the individual particles are also submicron in size and form compact clusters (Figure 8b). The relative abundance of the two morphologies is estimated to be approximately 70 : 30, with carbon nanosheets constituting the majority and spherical particle aggregates representing the minority phase. We thus assign the dominant broad reflection observed in the XRD pattern to the nanosheets, whereas the sharper, superimposed reflection is attributed to the secondary nanoparticle population.

Analogously to the titania case, ignition of the sugar-impregnated flash paper results in sheet-like carbon *via* a sacrificial templating effect imposed by the paper's lamellar architecture.[41] In parallel, volatile carbon-containing fragments generated during pyrolysis recombine and condense in the gas phase, forming irregular or near-spherical carbon particles.[42] Unlike cobalt blue,[14] which nucleates within transient molten droplets from low-melting precursor nitrate salts, carbon derived from sugar forms *via* solid-state and gas-phase pathways, resulting in distinct large, irregular or sheet-like structures under flash-combustion conditions. As mentioned earlier, the influence of flash paper thickness on particle size and morphology cannot be ruled out. Additional factors, such as local heating, the composition of the surrounding atmosphere, precursor concentration, and possible post-pyrolysis transformations like coalescence or restructuring, may further modulate carbon morphology and warrant future investigation.

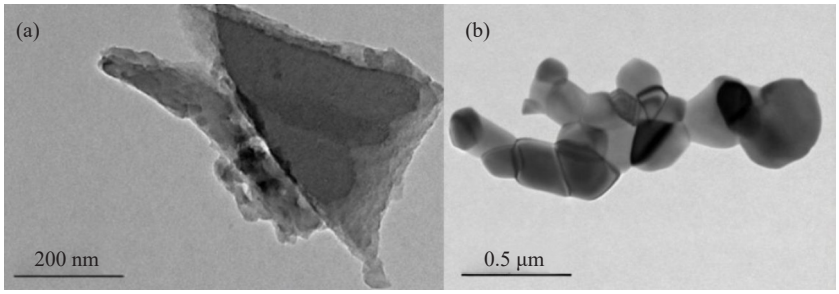

Figure 8. TEM images of the derived carbon, showing (a) nanosheets and (b) aggregates of nearly spherical particles

Carbon is a key component of black inks,[43,44] with roughly 100,000 metric tonnes used globally each year (primarily as carbon black pigment). These inks often contain 10% pigment dispersed in an acrylic binder, which stabilizes the pigment, ensures uniform film formation, and improves abrasion resistance.[45-47] Water serves as the primary carrier, offering a more environmentally friendly alternative to organic solvents.

Although most carbon black is sourced from hydrocarbon feedstocks,[1,10] carbon pigments derived from sugars are attracting growing interest for ink applications,[11-13] as they can be produced from inexpensive, widely available sugars *via* straightforward carbonization processes, making them highly cost-effective. Beyond low cost, they offer additional advantages such as tunable microstructure, good dispersibility in water-based formulations, and the potential for sustainable, bio-based sourcing. Their adaptable surface chemistry also allows easy functionalization, enabling compatibility with various printing techniques, which makes them attractive for scalable, eco-friendly ink development.

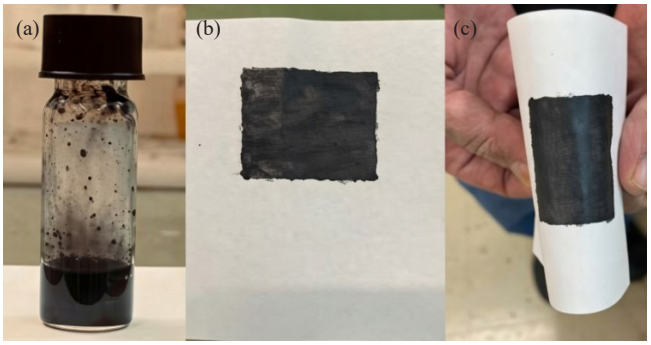

Figure 9. Carbon ink synthesized from sugar *via* flash-paper combustion, shown as a suspension (a) and as a dried, uniform coating on paper (b), demonstrating strong adhesion and flexibility upon bending (c)

Illustratively, carbon produced *via* flash-paper combustion was incorporated at 10% in a waterborne acrylic ink formulation (Figure 9a). When applied to paper, the ink formed a uniform black coating with a dense, consistent film (Figure 9b). The coating remained robust and flexible, showing no cracking or flaking when the paper was bent (Figure 9c). Overall, the images demonstrate the simplicity of the fabrication approach and the promising mechanical durability of the resulting carbon-based ink.

3.3 *Towards scalable flash-paper combustion for industrial pigment production*

In contrast to many conventional synthesis routes, which are typically energy-intensive and often rely on sophisticated, high-cost instrumentation, the present approach is intrinsically energy-releasing and operationally simple. Rather than requiring sustained external energy input, the process proceeds through self-sustaining reactions once initiated. This significantly reduces overall energy demand and eliminates the need for complex infrastructure. As a result, the method is particularly well suited for exploratory materials synthesis in decentralized or resource-limited settings, where access to advanced equipment and stable energy supply may be constrained.

However, translating this potential to an industrial scale would require a continuous, integrated workflow that would combine wet impregnation, controlled combustion, material collection, and energy recovery. In such a system, nitrocellulose sheets could be continuously passed through an aqueous precursor bath for impregnation and then dried in a multi-zone oven to ensure uniform moisture removal. The treated sheets would be precisely cut and fed into a pulse-controlled combustion chamber, where carefully timed ignitions would deliver rapid, controlled bursts of energy. The released heat could be captured *via* a water-jacketed heat exchanger to generate high-pressure steam for electricity production, while the pigments would be collected directly as the main product. By integrating impregnation, combustion management, and material/energy recovery into a single continuous process, this approach could provide a feasible pathway toward industrial-scale operation.[14]

4. Conclusions

The present work demonstrates that flash-paper combustion offers a versatile and rapid approach for synthesizing two important industrial pigments: titania and carbon. Titania was successfully produced by impregnating flash paper with a Ti(III) chloride solution and igniting it, yielding a lightweight powder composed of anatase and rutile phases. Subsequent calcination enabled near-complete conversion to rutile, which is suitable for pigment applications, as demonstrated by the effective coloration of lead borate glass. On the other hand, amorphous carbon pigment was generated by igniting sugar-impregnated flash paper. When blended into waterborne acrylic inks, the black pigment demonstrated uniform dispersion, flexibility, and strong adhesion. Beyond these practical demonstrations, this work additionally highlights the energy efficiency and self-sustaining nature of flash-paper combustion, which rapidly converts precursors into functional pigments while releasing thermal energy that could potentially be harnessed. The simplicity, speed, and potential scalability of the method suggest that it could be further developed for industrial

production of high-value pigments, offering a sustainable and cost-effective alternative to conventional synthesis routes. Finally, the approach could be readily expanded to produce metallic pigments and other products derived from nitrocellulose-based reactive scaffolds, such as flash cotton.

Acknowledgments

The authors gratefully acknowledge the UoI Network of Research Supporting Laboratories (NRSL) for providing access to XRD and TEM facilities. We also sincerely thank Dr. C. Papachristodoulou for assistance with the XRD measurements.

Conflict of interest

The authors have no conflict of interest to disclose.

References

[1] Buxbaum, G.; Pfaff, G. *Industrial Inorganic Pigments*, 3rd ed.; Wiley-VCH: Weinheim, 2005.
[2] Braun, J. H.; Baidins, A.; Marganski, R. E. TiO_2 pigment technology: A review. *Prog. Org. Coat.* **1992,** *20*, 105-138.
[3] Gázquez, M. J.; Bolívar, J. P.; Garcia-Tenorio, R.; Vaca, F. A review of the production cycle of titanium dioxide pigment. *Mater. Sci. Appl.* **2014,** *5*, 441-458.
[4] Chen, X.; Mao, S. S. Titanium dioxide nanomaterials: Synthesis, properties, modifications, and applications. *Chem. Rev.* **2007,** *107*, 2891-2959.
[5] Ghamarpoor, R.; Fallah, A.; Jamshidi, M. A review of synthesis methods, modifications, mechanisms of ZnO/TiO_2-based photocatalysts for photodegradation of contaminants. *ACS Omega* **2024,** *9*, 25457-25492.
[6] Siddique, F.; Gonzalez-Cortes, S.; Mirzaei, A.; Xiao, T.; Rafiq, M. A.; Zhang, X. Solution combustion synthesis: The relevant metrics for producing advanced and nanostructured photocatalysts. *Nanoscale* **2022,** *14*, 11806-11868.
[7] Khan, S.; Park, J.-S.; Ishihara, T. A review of the single-step flame synthesis of defective and heterostructured TiO_2 nanoparticles for photocatalytic applications. *Catalysts* **2023,** *13*, 196.
[8] Chalmpes, N.; Asimakopoulos, G.; Baikousi, M.; Bourlinos, A. B.; Karakassides, M. A.; Gournis, D. Hypergolic synthesis of inorganic materials by the reaction of metallocene dichlorides with fuming nitric acid at ambient conditions: The case of photocatalytic titania. *Sci* **2021,** *3*, 46.
[9] Mariño-Gámez, A. E.; Acosta-González, G.-E.; Pech-Canul, M. I.; Hernández, M. B.; García-Villarreal, S.; Zambrano-Robledo, P.; Barrios, B. S. V.; Aguilar-Martínez, J. A. Influence of high energy ball milling on structural, microstructural and optical properties of TiO_2 nanoparticles. *Ceram. Int.* **2022,** *48*, 3362-3367.
[10] Pfaff, G. Carbon black pigments. *Phys. Sci. Rev.* **2022,** *7*, 109-125.
[11] Goh, Y.; Lauro, S.; Barber, S. T.; Williams, S. A.; Trabold, T. A. Cleaner production of flexographic ink by substituting carbon black with biochar. *J. Clean. Prod.* **2021,** *324*, 129262.
[12] Li, X.; Zeng, J.; Zuo, S.; Lin, S.; Chen, G. Preparation, modification, and application of biochar in the printing field: A review. *Materials* **2023,** *16*, 5081.
[13] Elmaghraby, N. A.; Hassaan, M. A.; Zien, M. A.; Abedelrhim, E. M.; Ragab, S.; Yılmaz, M.; El Nemr, A. Fabrication of carbon black nanoparticles from green algae and sugarcane bagasse. *Sci. Rep.* **2024,** *14*, 5542.
[14] Bourlinos, A. B.; Polymeros, A.; Papachristodoulou, C.; Moschovas, D.; Avgeropoulos, A.; Salmas, C. E.; Karakassides, M. A. Rapid flash paper combustion synthesis of cobalt blue pigment nanoparticles for use in color 3D printing formulations. *Appl. Funct. Mater.* **2025,** *5*, 19-30.
[15] Pecsok, R. L.; Fletcher, A. N. Hydrolysis of titanium(III). *Inorg. Chem.* **1962,** *1*, 155-159.
[16] Cassaignon, S.; Koelsch, M.; Jolivet, J.-P. From $TiCl_3$ to TiO_2 nanoparticles (anatase, brookite and rutile): Thermohydrolysis and oxidation in aqueous medium. *J. Phys. Chem. Solids* **2007,** *68*, 695-700.
[17] Morris, E.; Pulham, C. R.; Morrison, C. A. Structure and properties of nitrocellulose: Approaching 200 years of research. *RSC Adv.* **2023,** *13*, 32321-32333.

[18] Hanaor, D. A. H.; Sorrell, C. C. Review of the anatase to rutile phase transformation. *J. Mater. Sci.* **2011,** *46*, 855-874.
[19] Wilke, T.; Schneider, M.; Kleinermanns, K. 1,4-Hydroquinone is a hydrogen reservoir for fuel cells and recyclable via photocatalytic water splitting. *Open J. Phys. Chem.* **2013**, *3*, 97-102.
[20] Jin, Y.-S.; Wang, P.; Teng, S.-H. Hexafluorotitanic acid-assisted synthesis of large-sized, ultrathin titania nanosheets as multifunctional and high-performance photocatalysts. *Nanotechnology* **2020,** *31*, 405605.
[21] Yu, H.; Tian, B.; Zhang, J. Layered TiO_2 composed of anatase nanosheets with exposed {001} facets: Facile synthesis and enhanced photocatalytic activity. *Chem. Eur. J.* **2011,** *17*, 5499-5502.
[22] Zhang, Q.-S.; Li, Q.-L.; Li, J.-Q.; Bai, R. Photocatalysis of TiO_2 sheets prepared by templating filter paper. *Chin. J. Chem. Phys.* **2011,** *24*, 85-90.
[23] Arvan, B.; Khakifirooz, A.; Tarighat, R.; Mohajerzadeh, S.; Goodarzi, A.; Soleimani, E. A.; Arzi, E. Atmospheric pressure chemical vapor deposition of titanium dioxide films from $TiCl_4$. *Mater. Sci. Eng. B* **2004**, *109*, 17-23.
[24] Singh, D.; Singh, K.; Singh, G.; Manupriya; Mohan, S.; Arora, M.; Sharma, G. Optical and structural properties of ZnO-PbO-B_2O_3 and ZnO-PbO-B_2O_3-SiO_2 glasses. *J. Phys.: Condens. Matter* **2008,** *20*, 075228.
[25] Shalaby, A.; Aleksandrov, L.; Iordanova, R.; Staneva, A.; Dimitriev, Y. Synthesis and characterization of glass doped reduced graphene oxide. *J. Chem. Technol. Metall.* **2015,** *50*, 474-477.
[26] Jana, S.; Karmakar, B.; Kundu, P. Unusual visible absorption in high PbO lead borate glass. *Mater. Sci.-Pol.* **2007,** *25*, 1127-1134.
[27] Maltsev, S.; Dymshits, O.; Alekseeva, I.; Volokitina, A.; Tenevich, M.; Bachina, A.; Bogdanov, K.; Zapalova, S.; Shakhgildyan, G.; Zhilin, A. Glass-ceramics of the lithium aluminosilicate system nucleated by TiO_2: The role of redox conditions of glass melting in phase transformations and properties. *Material*s **2025,** *18*, 785.
[28] Chavoutier, M.; Caurant, D.; Majérus, O.; Boulesteix, R.; Loiseau, P.; Jousseaume, C.; Brunet, E.; Lecomte, E. Effect of TiO_2 content on the crystallization and the color of (ZrO_2, TiO_2)-doped Li_2O-Al_2O_3-SiO_2 glasses. *J. Non-Cryst. Solids* **2014,** *384*, 15-24.
[29] Karlsson, S.; Bäck, L. G.; Kidkhunthod, P.; Lundstedt, K.; Wondraczek, L. Effect of TiO_2 on optical properties of glasses in the soda-lime-silicate system. *Opt. Mater. Express* **2016,** *6*, 1198-1216.
[30] Meechoowas, E.; Pantulap, U.; Jitwatcharakomal, T. Investigation of the properties of soda-lime silicate glass doped with TiO_2. *Adv. Mater. Res.* **2014,** *979*, 128-131.
[31] Kirdsiri, K.; Srisittipokakun, N.; Ruangtaweep, Y.; Boonin, K.; Limsuwan, P.; Kaewkhao, J. Effect of addition TiO_2 on Bi_2O_3-TiO_2-B_2O_3 glasses. *Adv. Mater. Res.* **2013,** *770*, 72-75.
[32] Yu, L.; Falco, C.; Weber, J.; White, R. J.; Howe, J. Y.; Titirici, M.-M. Carbohydrate-derived hydrothermal carbons: a thorough characterization study. *Langmuir* **2012,** *28*, 12373-12383.
[33] Wortmann, M.; Keil, W.; Brockhagen, B.; Biedinger, J.; Westphal, M.; Weinberger, C.; Diestelhorst, E.; Hachmann, W.; Zhao, Y.; Tiemann, M.; et al. Pyrolysis of sucrose-derived hydrochar. *J. Anal. Appl. Pyrol.* **2022,** *161*, 105404.
[34] Baer, H. H.; Chiu, S.-H. L. The synthesis of nitro and dimeric nitroso sugars by peracid oxidation of amino sugars. *Can. J. Chem.* **1973,** *51*, 1812-1818.
[35] Heyns, K.; Roper, S.; Roper, H.; Meyer, B. N-nitroso sugar amino acids. *Angew. Chem. Int. Ed. Engl.* **1979,** *18*, 878-880.
[36] Qi, Y.; Wei, D.; Shi, G.-M.; Zhang, M.; Qi, Y. Amorphous/nanocrystalline carbonized hydrochars with isomeric heterogeneous interfacial polarizations for high-performance microwave absorption. *Sci. Rep.* **2019,** *9*, 12429.
[37] Ilkiv, B.; Petrovska, S.; Sergiienko, R.; Foya, O.; Ilkiv, O.; Shibata, E.; Nakamura, T.; Zaulychnyy, Y. Electronic structure of hollow graphitic carbon nanoparticles fabricated from acetylene carbon black. *Fuller. Nanotub. Carbon Nanostruct.* **2014,** *23*, 449-454.
[38] Thapliyal, V.; Alabdulkarim, M. E.; Whelan, D. R.; Mainali, B.; Maxwell, J. L. A concise review of the Raman spectra of carbon allotropes. *Diam. Relat. Mater.* **2022,** *127*, 109180.
[39] Fathy, M.; Moghny, T. A.; Mousa, M. A.; El-Bellihi, A.-H. A.-A.; Awadallah, A. E. Absorption of calcium ions on oxidized graphene sheets and study its dynamic behavior by kinetic and isothermal models. *Appl. Nanosci.* **2016**, *6*, 1105-1117.
[40] Singh, M.; Vander Wal, R. L. Nanostructure quantification of carbon blacks. *C* **2019,** *5*, 2.
[41] Son, S.-Y.; Yang, S.-L.; Lee, S.; Na, S.-I.; Joh, H.-I. Eco-friendly cellulose-derived transparent carbon nanosheet electrodes. *Mater. Res. Bull.* **2020,** *132*, 110999.
[42] Bourlinos, A. B.; Georgakilas, V.; Zboril, R. Easy deposition of amorphous carbon films on glass substrates. *Carbon* **2008,** *46*, 1801-1804.
[43] Ali, M.; Lin, L.; Faisal, S.; Ali, S. R.; Ali, S. I. Let-down stability and screen printability of inks prepared using

non-printing ink grades of carbon black pigment. *Pigm. Resin Technol.* **2019,** *48*, 523-532.
[44] Kassim, A. D.; Emmanuel, I. The production and optimization of printing ink derived from waste tire carbon black. *Int. J. Res. Sci. Innov.* **2025,** *12*, 453-461.
[45] Tauber G, Batz-Sohn C, Nelli L, McIntosh R, Kalbitz W. Improved dispersibility of surface oxidized carbon black pigments for inkjet ink formulation. In *Proceedings of the 26th International Conference on Digital Printing Technologies and Digital Fabrication (NIP26)*; Springfield (VA): Society for Imaging Science and Technology, 2010; pp 181-184.
[46] Kuo, C.-H.; Shiu, J.-W.; Rwei, S.-P. Preparation and characterization of PMMA encapsulated carbon black for water-based digital jet printing ink on different fibers of cotton and PET. *Colloids Surf. A* **2022,** *648*, 129450.
[47] Mesa, S.; Ramírez, E.; Botia, K. G. R.; Jaramillo, F.; Ramírez, D. Development and characterization of carbon-based conductive pastes with high mechanical integrity under bending stress for room-temperature printable electronics. *Sci. Rep.* **2025,** *15*, 6397.